

## Supplementary Information

# **Nickel-Borate with 3D Hierarchical Structure as a Robust and Efficient Electrocatalyst for Urea Oxidation**

*Jianhua Ge, Yuecheng Lai, Minghui Guan, Yuhua Xiao, Juner Kuang, Chunzhen Yang\**

School of Materials, Sun Yat-sen University, Guangzhou, 510275, China

\*Corresponding Author: [yangchzh6@mail.sysu.edu.cn](mailto:yangchzh6@mail.sysu.edu.cn)

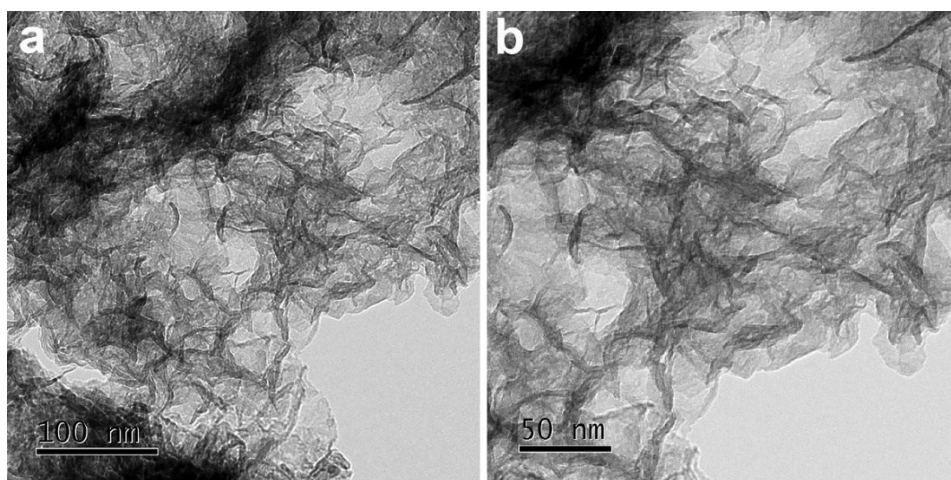


**Fig. S1** TEM images showing the morphology of Ni-B<sub>i</sub> catalyst.

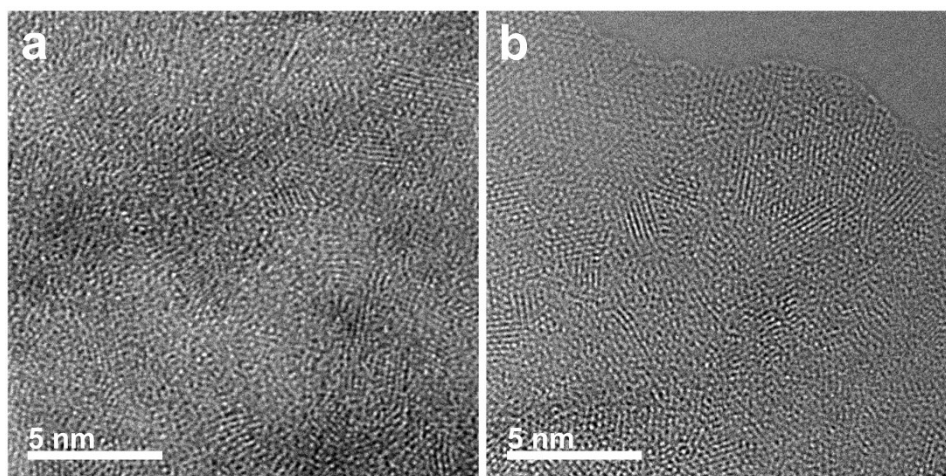


**Fig. S2** HR-TEM images of Ni-B<sub>i</sub> catalyst.

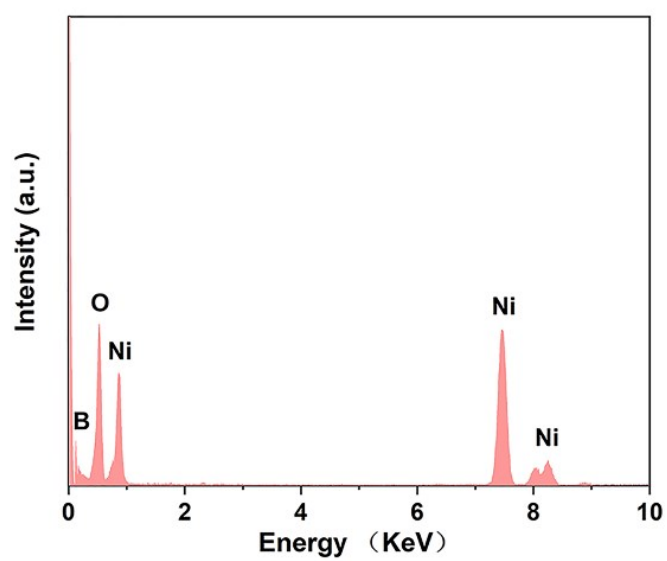


Fig. S3 EDX spectrum for Ni-B<sub>1</sub>.

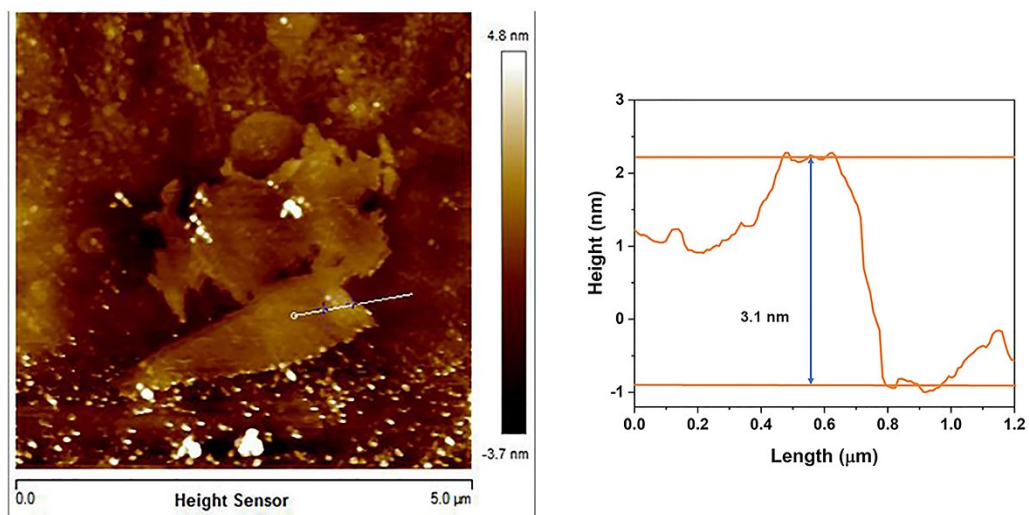


Fig. S4 Atomic force microscopy (AFM) images and height profiles of Ni-B<sub>1</sub> nanosheet.

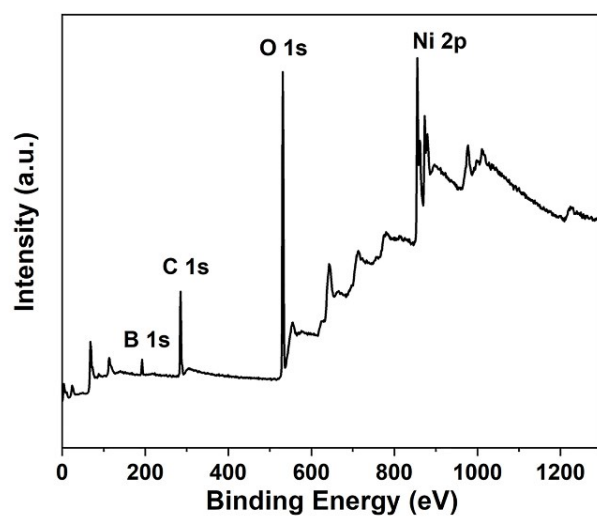


Fig. S5 XPS spectrum of Ni-B<sub>i</sub>.

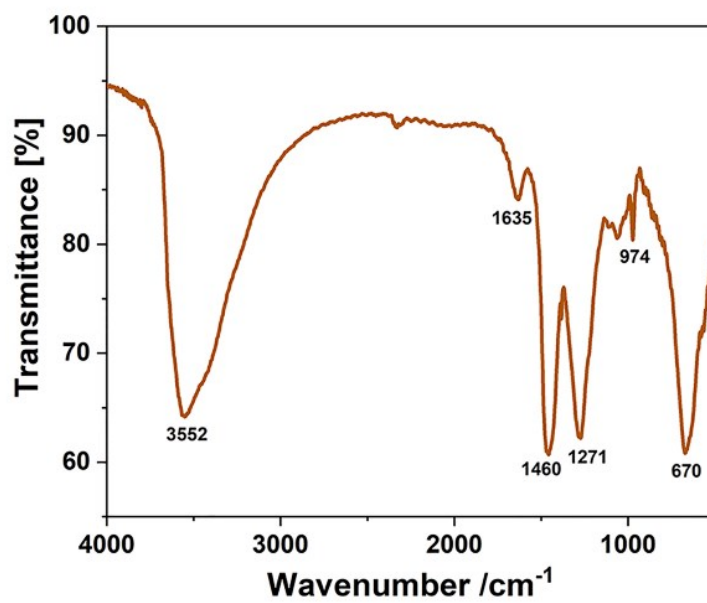
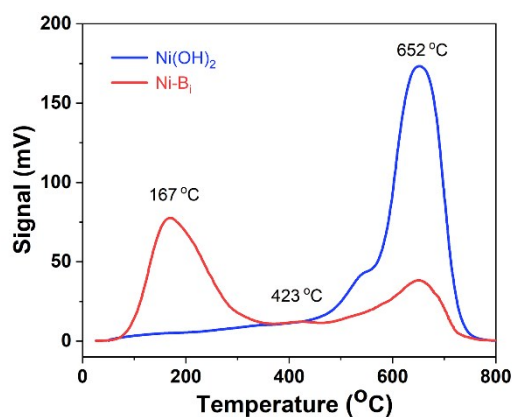


Fig. S6 FT-IR spectra of the Ni-B<sub>i</sub> catalyst



**Fig. S7** CO<sub>2</sub>-TPD spectra of Ni-B<sub>1</sub> and Ni(OH)<sub>2</sub>.

For the CO<sub>2</sub>-TPD experiment, the Ni-B<sub>1</sub> or Ni(OH)<sub>2</sub> powder sample was placed in a quartz cell, degassing with N<sub>2</sub> at 150 °C for 1 h. After the sample is cooling down to room temperature, the quartz cell was filled with CO<sub>2</sub> gas for CO<sub>2</sub> absorption for 1h. During the CO<sub>2</sub> desorption reaction, the cell temperature was raised at a heating rate of 10 °C/min to 800 °C.

According to Figure S7, large amount of CO<sub>2</sub> is desorbed from the surface of Ni-B<sub>1</sub> powder at low temperature, which is a strong indication for the present of enriched active Ni sites on the Ni-B<sub>1</sub> catalyst. In addition, the initial temperature for CO<sub>2</sub> desorption from Ni-B<sub>1</sub> is much lower than that of the Ni(OH)<sub>2</sub>. Therefore, it's concluded that the desorption energy involved for CO<sub>2</sub> removal from Ni-B<sub>1</sub> is much lower, which may be responsible for the fast kinetics in urea catalysis.

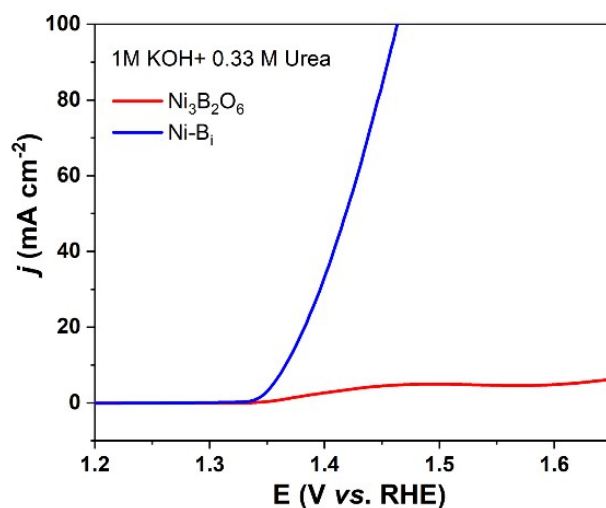


**Fig. S8** Comparison of UOR activity of Ni-B<sub>1</sub> and Ni<sub>3</sub>B<sub>2</sub>O<sub>6</sub>.

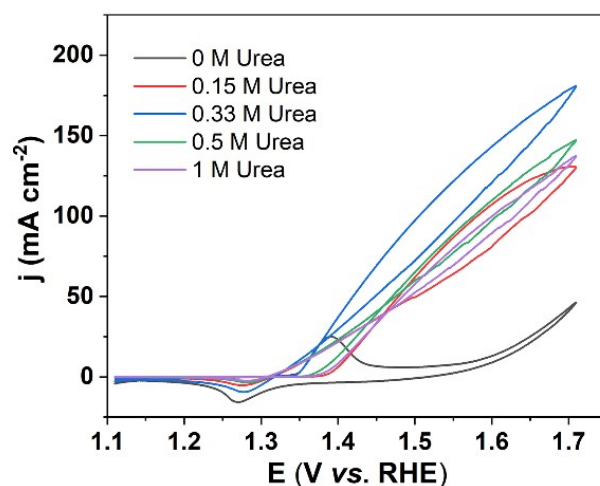


**Fig. S9** The UOR performance of Ni-B<sub>1</sub> catalyst in different urea concentrations.

The UOR experiments are conducted with a selected urea concentration of 0.33 M, which is based on the approximate concentration of urea in human urine and most of the references reported in previous literatures. We also tried to optimize the UOR performance by varying the urea concentrations in  $\sim$ 1M KOH at a fixed pH=14. As shown in Fig. S9, the anodic current obtained at 1.45 V vs. RHE for UOR cannot be further enhanced at increased urea concentrations. At higher concentrations, the UOR activity decreases because the active sites of Ni-B<sub>1</sub> maybe fully covered by adsorbed urea molecules or reaction intermediates, with poor accessibility of OH<sup>-</sup> anions for efficient PCET steps.

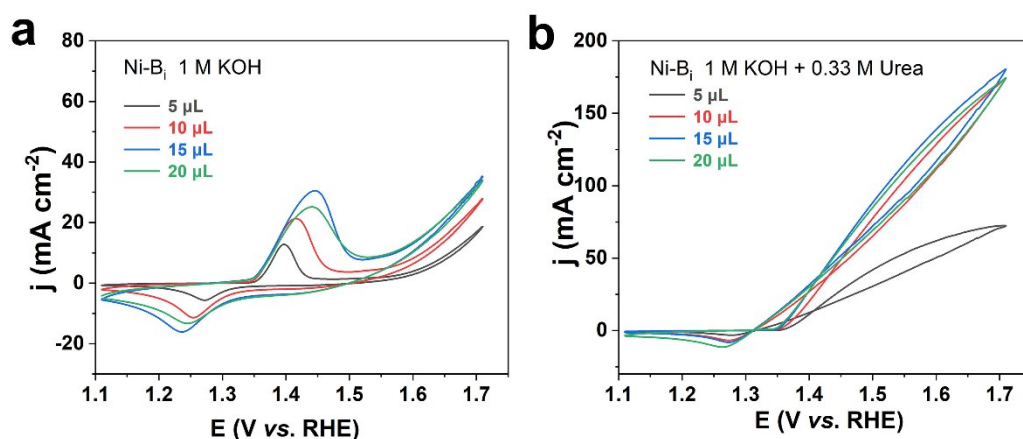


**Fig. S10** Effect of Ni-Bi's loading account on OER and UOR performance.

The UOR performance is examined by varying the loading amount of Ni-Bi catalyst on the glassy carbon electrode, from  $\sim 130 \mu\text{g cm}^{-2}$  (drop casting of 5  $\mu\text{L}$  catalyst ink) to  $\sim 520 \mu\text{g cm}^{-2}$  (drop casting of 20  $\mu\text{L}$  catalyst ink).

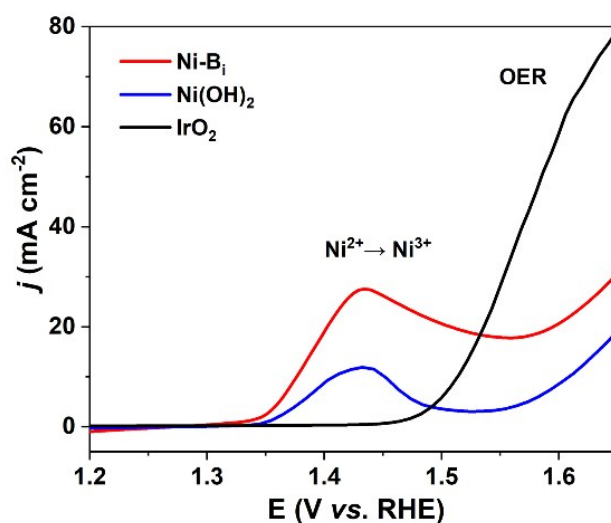


**Fig. S11** Comparison of the OER activities of Ni-Bi, Ni(OH)<sub>2</sub> and IrO<sub>2</sub> in 1.0 M KOH

According to the LSV polarization curves of the electrochemical oxidation of the catalysts, the Ni-Bi sample clearly possessed larger amount of exposed Ni sites that are electrochemically accessible by the electrolyte. The anodic peak in the potential range of 1.35 ~1.55 V vs. RHE shows the transformation of Ni<sup>2+</sup> to Ni<sup>3+</sup>, and the peak area of the Ni-Bi catalyst is estimated to be  $\sim 3$  times higher than that of Ni(OH)<sub>2</sub>.

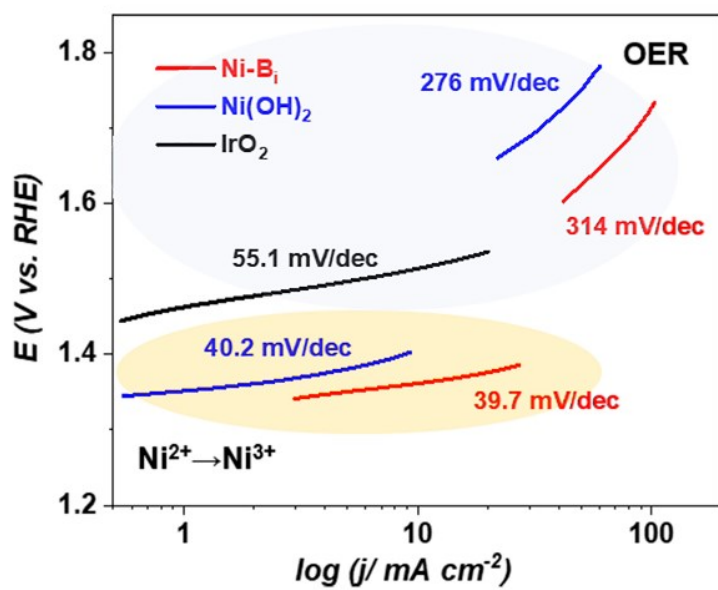


**Fig. S12** Tafel plots of Ni-B<sub>i</sub>, Ni(OH)<sub>2</sub> and IrO<sub>2</sub> in 1.0 M KOH

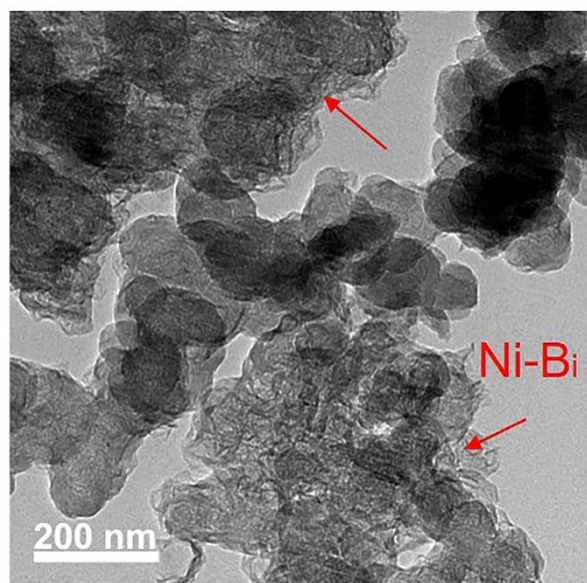


**Fig. S13** TEM images of Ni-B<sub>i</sub> catalyst after the UOR stability test. Arrows point out the Ni-B<sub>i</sub> nanosheets.

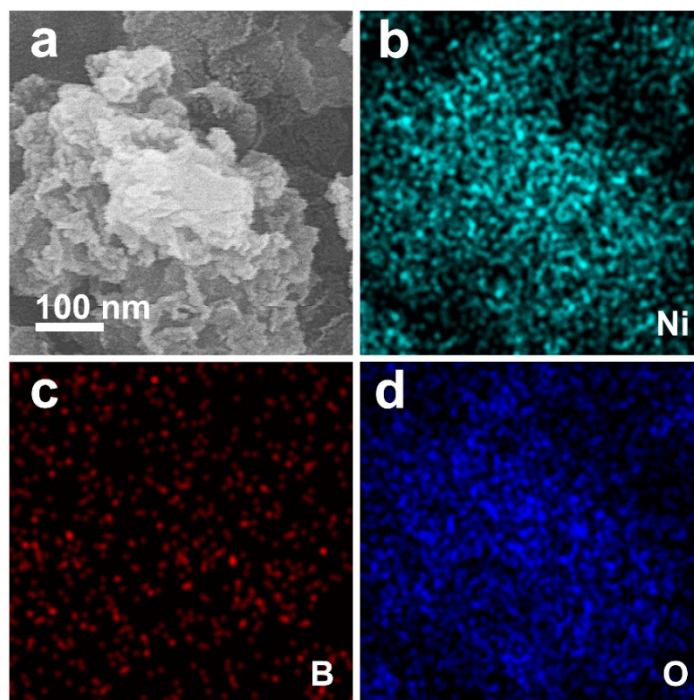


**Fig. S14** (a) SEM-EDX mapping images of Ni-B<sub>i</sub> catalyst after UOR stability test, and element mapping of (b) Ni, (c) B, (d) O.

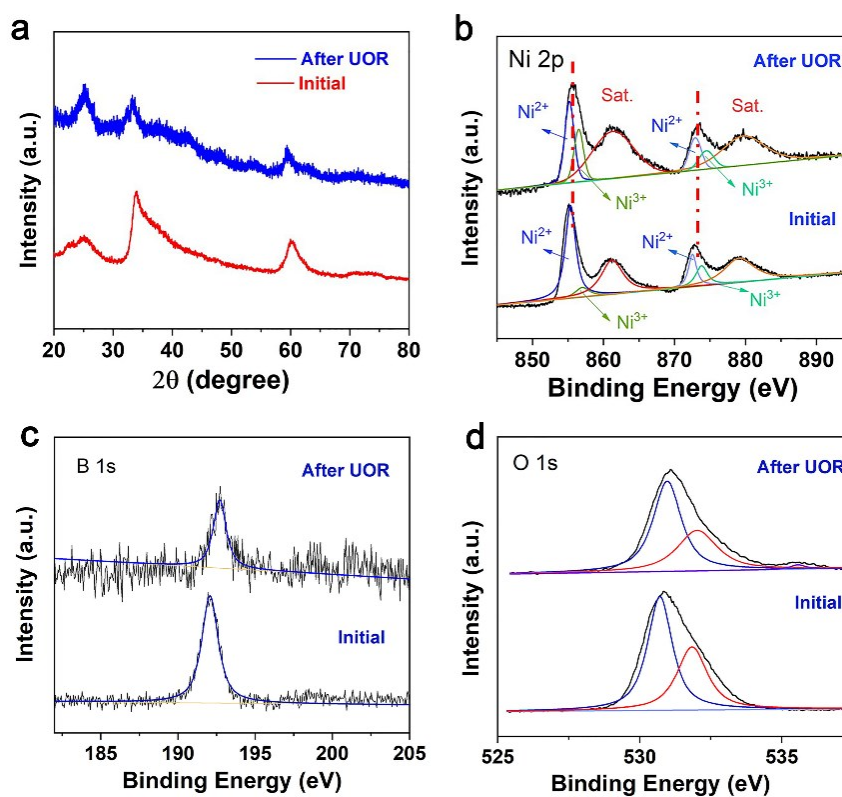


**Fig. S15** (a) XRD and (b) XPS spectra of the cycled Ni-B<sub>i</sub> catalyst after UOR stability test.

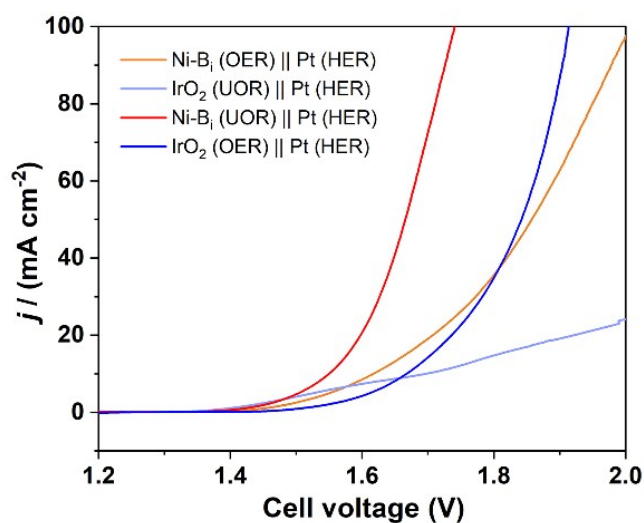


**Fig. S16** Comparison of polarization curves using IrO<sub>2</sub> and Ni-B<sub>i</sub> as the anodic catalyst in 1.0 M KOH solution for water electrolysis, or in 1.0 M KOH solution with 0.33 M urea for urea electrolysis.

We compared four different catalyst systems for hydrogen generation using two-electrode configuration in a H-type electrolyzer cell with two chambers separated by a Nafion membrane. As shown in Figure S18, when using Ni-B<sub>i</sub> as the anodic electrode for UOR and Pt as the cathodic electrode for HER, the electrolyzer cell can deliver the highest current (red curve). Results suggested that the combination of Ni-B<sub>i</sub> (for UOR) and Pt (for HER) is a prominent catalyst system for efficient hydrogen production.

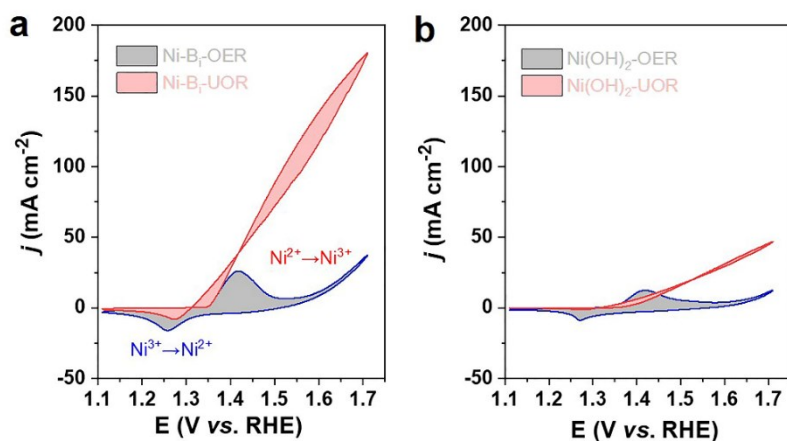


**Fig. S17** CV curves of Ni-B<sub>i</sub> and Ni(OH)<sub>2</sub> in 1.0 M KOH solution with and without 0.33 M urea.

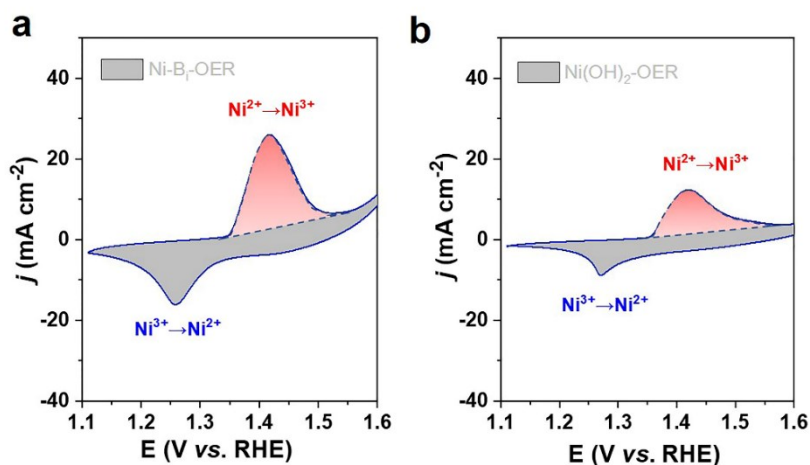


**Fig. S18** Oxidation of Ni<sup>2+</sup> to Ni<sup>3+</sup> during the anodic scan for (a) Ni-B<sub>i</sub> and (b) Ni(OH)<sub>2</sub>.

The activity of Ni-B<sub>i</sub> catalyst was also expressed in turnover frequencies (TOFs), based on the active sites estimated from the anodic CV curves that revealed the active Ni sites accessible for electrochemical reaction. The TOF can be calculated by the equation

$$TOF = \frac{J \cdot A}{6 \cdot F \cdot m}$$

where J is the anodic current density at certain overpotential, A the geometrical surface area of the electrode, F the Faraday constant (96485 C/mol), and m the amount of dimeric active sites, which equals the Ni loading, as estimated by the redox peak in the CV. 6 equivalent of electrons are involved in the electrochemical oxidation of one mole urea molecules. Based on the Ni content calculated from the total charge of the Ni<sup>2+</sup>/Ni<sup>3+</sup> redox wave in the cyclic voltammogram (CV; Fig. S18), the TOF at 1.55 V vs. RHE for UOR was calculated to be about 4.03 s<sup>-1</sup> for Ni-Bi catalyst and 2.74 s<sup>-1</sup> for

Ni(OH)<sub>2</sub>, whereas the TOF for OER is estimated to be 0.18 s<sup>-1</sup> for Ni-B<sub>i</sub>, and 0.27 s<sup>-1</sup> for Ni(OH)<sub>2</sub>.

**Table S1** Atomic ratios of Ni-B<sub>i</sub> determined by XPS

Name	Start BE	Peak BE	End BE	Height CPS	FWHM eV	Area(p) CPS. eV	Area(N)	Atomic %
C 1s	293.43	284.79	279.38	18893.76	1.53	39596.06	555.23	26.6
B 1s	204.23	192.08	180.38	3842.58	1.43	8937.24	314.34	15.06
O 1s	545.18	530.89	525.48	64548	2.15	153356.58	888.95	42.59
Ni 2p	895.28	855.18	844.38	39522.88	2.44	300863.92	328.72	15.75

**Table S2** Electrochemical impedance parameters estimated from the fitted data impedance spectra of Ni-B<sub>i</sub> at different applied potential.

Potential (V vs. RHE)	R <sub>s</sub> (ohm)	R <sub>ct1</sub> (ohm)	R <sub>ct2</sub> (ohm)
1.35	4.65	3.261	8.601
1.4	4.68	3.685	5.767
1.45	4.7	4.222	3.768
1.5	4.73	4.596	5.1
1.55	4.9	4.348	7.522
1.6	5.1	6.5	9.05

**Table S3** Comparison of UOR activity of Ni-B<sub>i</sub> and other electrocatalysts.

Electrocatalysts	Electrolyte	Potential (V)	Current Density (mA cm <sup>-2</sup> )	Ref.
Ni-B <sub>i</sub>	1.0 M KOH 0.33 M urea	1.35	10	This work
Ni <sub>2</sub> P	1.0 M KOH 0.33 M urea	1.38	10	2
Ni <sub>2</sub> P/Fe <sub>2</sub> P	1.0 M KOH 0.5 M urea	1.344	10	3
Ni(OH) <sub>2</sub> @NF	1.0 M KOH 0.33 M urea	1.35	10	4
Ni-WO <sub>2</sub> @C/NF	1.0 M KOH 0.33 M urea	1.31	10	5
Ni-MOF	1.0 M KOH 0.33 M urea	1.36	10	6
Ni-Fe LDH	1.0 M KOH 0.5 M urea	1.335	10	7
MnO <sub>2</sub> /MnCo <sub>2</sub> O <sub>4</sub> /Ni	1.0 M KOH 0.5 M urea	1.33	10	8
Ni-Mo	1.0 M KOH 0.33 M urea	1.36	10	9
Ni-Fe LDH	1.0 M KOH 0.33 M urea	1.362	30	10
Fe:α-Ni(OH) <sub>2</sub>	1.0 M KOH 0.33 M urea	1.408	100	11
Cu:α-Ni(OH) <sub>2</sub>	1.0 M KOH 0.33 M urea	1.405	100	12

## Reference :

- 1 Y. Yanagisawa, K. Takaoka, S. Yamabe and T. Ito, Interaction of CO<sub>2</sub> with Magnesium Oxide Surfaces: a TPD, FTIR, and Cluster-Model Calculation Study, *J. Phys. Chem.*, 1995, **99**, 3704-3710.
- 2 X. Zhang, Y. Liu, Q. Xiong, G. Liu, C. Zhao, G. Wang, Y. Zhang, H. Zhang and H. Zhao, Vapour-phase hydrothermal synthesis of Ni<sub>2</sub>P nanocrystallines on carbon fiber cloth for high-efficiency H<sub>2</sub> production and simultaneous urea decomposition, *Electrochim. Acta*, 2017, **254**, 44-49.
- 3 H. Xu, K. Ye, K. Zhu, Y. Gao, J. Yin, J. Yan, G. Wang and D. Cao, Transforming Carnation-Shaped MOF-Ni to Ni-Fe Prussian Blue Analogue Derived Efficient Bifunctional Electrocatalyst for Urea Electrolysis, *ACS Sustain. Chem. & Eng.*, 2020, **8**, 16037-16045.
- 4 L. Xia, Y. Liao, Y. Qing, H. Xu, Z. Gao, W. Li and Y. Wu, In Situ Growth of Porous Ultrathin Ni(OH)<sub>2</sub> Nanostructures on Nickel Foam: An Efficient and Durable Catalysts for Urea Electrolysis, *ACS Appl. Energy Mater.*, 2020, **3**, 2996-3004.
- 5 F. Shen, W. Jiang, G. Qian, W. Chen, H. Zhang, L. Luo and S. Yin, Strongly coupled carbon encapsulated Ni-WO<sub>2</sub> hybrids as efficient catalysts for water-to-hydrogen conversion via urea electro-oxidation, *J. Power Sources*, 2020, **458**, 228014.
- 6 D. Zhu, C. Guo, J. Liu, L. Wang, Y. Du and S.-Z. Qiao, Two-dimensional metal-organic frameworks with high oxidation states for efficient electrocatalytic urea oxidation, *ChemComm*, 2017, **53**, 10906-10909.
- 7 X. Wen, NiFe-LDH/MWCNTs/NF nanohybrids as a high-performance bifunctional electrocatalyst for overall urea electrolysis, *Int. J. Hydrog. Energy*, 2020, **45**, 14660-14668.
- 8 C. Xiao, S. Li, X. Zhang and D. R. MacFarlane, MnO<sub>2</sub>/MnCo<sub>2</sub>O<sub>4</sub>/Ni heterostructure with quadruple hierarchy: a bifunctional electrode architecture for overall urea oxidation, *J. Mater. Chem. A*, 2017, **5**, 7825-7832.
- 9 J.-Y. Zhang, T. He, M. Wang, R. Qi, Y. Yan, Z. Dong, H. Liu, H. Wang and B. Y. Xia, Energy-saving hydrogen production coupling urea oxidation over a bifunctional nickel-molybdenum nanotube array, *Nano Energy*, 2019, **60**, 894-902.
- 10 J. Xie, H. Qu, F. Lei, X. Peng, W. Liu, L. Gao, P. Hao, G. Cui and B. Tang, Partially amorphous nickel-iron layered double hydroxide nanosheet arrays for robust bifunctional electrocatalysis, *J. Mater. Chem. A*, 2018, **6**, 16121-16129.
- 11 J. Xie, W. Liu, F. Lei, X. Zhang, H. Qu, L. Gao, P. Hao, B. Tang and Y. Xie, Iron-Incorporated  $\alpha$ -Ni(OH)<sub>2</sub> Hierarchical Nanosheet Arrays for Electrocatalytic Urea Oxidation, *Chem.- Eur.*, 2018, **24**, 18408-18412.
- 12 J. Xie, L. Gao, S. Cao, W. Liu, F. Lei, P. Hao, X. Xia and B. Tang, Copper-incorporated hierarchical wire-on-sheet  $\alpha$ -Ni(OH)<sub>2</sub> nanoarrays as robust trifunctional catalysts for synergistic hydrogen generation and urea oxidation, *J. Mater. Chem. A*, 2019, **7**, 13577-13584.